FULL-WAVE SIMULATION OF THE FORWARD SCATTER RADAR CROSS-SECTION FOR UAV DETECTION

Ivan Bokhan, Oleksii Bielousov, Vasyl Lykhograi, Dmytro Gavva

Department of Computer Radio Engineering and Technical Information Security Systems, Physical Foundations of Electronic Engineering Department
Kharkiv National University Of Radio Electronics, Ukraine.

E-mail: ivan.bokhan@nure.ua,
oleksii.bielousov@nure.ua ,
vasyl.lykhograi@nure.ua,
dmytro.gavva@nure.ua

Abstract

This study investigates the characteristics of forward scattering of electromagnetic waves from objects with different geometric shapes, aiming to determine their forward scatter cross-section (FSCS). Numerical simulations were performed for the illumination of individual faces and three-dimensional surfaces of geometric models, including a parallelepiped and an ogive-shaped body, representing typical configurations of small aerial vehicles. The study demonstrates that, in the forward-scatter regime, the dominant factor influencing the FSCS is the geometric projection of the target onto the plane perpendicular to the incident wave direction. This results in a significant increase in the scattered signal compared to the classical monostatic RCS. The obtained results confirm the high sensitivity of FSR systems to small-sized objects and can be applied to the optimization of passive radar fences, UAV detection systems, and signature assessment of advanced aerodynamic shapes.

With the establishment of radar as a distinct field of knowledge, most radar systems have adopted a configuration in which the transmitter and receiver are co-located – the so-called monostatic radars, where the processing involves electromagnetic (EM) fields/waves reflected or backscattered from objects/targets. Another example is bistatic radar, where the transmitter and receiver are placed at different locations, enabling the observation of EM fields/waves scattered by the target in directions other than directly back toward the transmitter, as in the monostatic configuration. Typically, bistatic radars measure the time difference between the transmitted signal and the echo received from the target, as well as the frequency difference caused by the Doppler shift [1].

The reasons why bistatic radars have not gained widespread adoption are primarily related to higher costs – including R&D and operational expenses – associated with the transmitter and receiver equipment, which are spatially separated, as well as the required network infrastructure. In addition, bistatic systems involve more complex algorithms for target detection, localization, and data processing in general.

However, in recent years, there has been a renewed interest in bistatic radar systems, primarily driven by the emergence of a wide range of affordable Software-Defined Radio (SDR) platforms and the rapid development of Passive Coherent Location (PCL) systems, in which bistatic radar configurations are implemented using third-party radiation sources, known as Illuminators of Opportunity (IoO) [1].

The geometry of a bistatic radar is illustrated in Fig. 1. It is described by a bistatic triangle with vertices located at the positions of the transmitter T, the receiver R, and the observed object or target O. The target is situated at a distance $|TO|$ from the transmitter and at a distance $|OR|$ from the receiver. The angle β between the sides $|TO|$ and $|OR|$ of the bistatic triangle is a key parameter and is referred to as the bistatic angle.

A special case exists in the bistatic radar configuration when $|TO| + |OR| \approx |TR|$, in which the bistatic angle β is approximately 180 degrees. The line-of-sight path $|TR|$ between the transmitter and the receiver is commonly referred to as the baseline. Thus, when the bistatic angle $\beta \approx 180°$, the object or target lies on or near the baseline. This configuration is known as Forward Scatter Radar (FSR). In the literature, FSR systems are also referred to as line radar, electronic fences or barriers, and flutter radar [1].

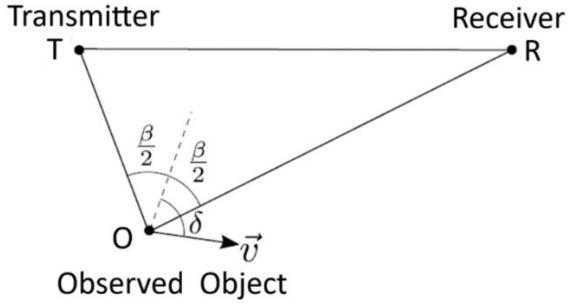

Fig. 1. Geometry of a Bistatic Radar

For a target located on the baseline, the size of the range resolution cell approaches infinity, and the echo signal from a moving object – regardless of its speed – always exhibits zero Doppler frequency shift f_D at the receiver. Therefore, an FS radar does not provide range resolution, since all scattered signals from targets located anywhere along the baseline arrive at the receiving antenna simultaneously. Consequently, FS radar does not provide velocity resolution either.

Despite these limitations, the geometry of an FS radar offers a significant advantage: the dominant physical principle underlying target observation is the phenomenon of forward scattering (FS) of the EM field/waves, as opposed to backscattering, which is typical for monostatic and bistatic radar systems.

Forward scattering arises from coherent phase perturbations of the EM field/waves in the shadow region of the target, where interference leads to a focusing of the field along a line perpendicular to the shadow area. When the target crosses the transmitter–receiver line, it partially blocks the incident wave from the IoO, generating a diffraction shadow. At this moment, the signal at the FS receiver increases sharply due to the formation of a narrow diffraction FS peak – the so-called FS maximum.

This makes FSR particularly sensitive to small-sized objects and changes in their position. As a result, the signal-to-noise ratio (SNR) in FSR systems can be an order of magnitude higher than in conventional monostatic radars [2].

Thus, the phenomenon of forward scattering is accompanied by a significant increase in the radar cross-section (RCS) of the object or target. In this regime, the amount of scattered energy is primarily determined by the geometric projection of the object onto a plane perpendicular to the direction of wave incidence and is almost independent of the material properties or viewing angle. The increase in RCS in the forward-scatter region enables the use of FS radars for detecting small-sized targets or extending the detection range. These factors are the primary reason for the growing interest in FSR systems today. Additionally, the forward scattering effect depends on the shadow area of the object or target and is independent of its material composition, which makes it possible to detect stealth objects that typically remain undetectable to monostatic radars.

Thus, it can be assumed that low-signature objects – such as quadcopters, small-sized UAVs, and stealth targets – are capable of producing a clearly measurable and strong diffraction silhouette in an FS radar system, and can therefore be detected.

In traditional radar systems, the level of the echo signal is determined by the RCS of the target. For both monostatic (σ_M) and bistatic (σ_B) radar configurations, the RCS is measured in square meters (m²) or decibel-square meters (dB·m²), and is defined as follows [1]:

$$\sigma = \lim_{R\to\infty} 4\pi R^2 \frac{|E_{sc}|^2}{|E_{inc}|^2} [m^2] \quad (1)$$

where E_{inc} is the electric field strength of the incident wave at the target location; E_{sc} is the electric field strength of the scattered wave in the direction of the observation point; and R is the distance from the observation point to the target.

In FS radars, a similar parameter is used – σ_{FS}, the forward scatter radar cross-section (Forward Scatter Cross-Section, FSCS). The FSCS characterizes the signal level of the shadow-region radiation field produced by an object with a shadow area S_B, as observed by an FS receiver located in the far field of the target. It is given by the following expression:

$$\sigma_{FS} = 4\pi \left(\frac{S_B}{\lambda}\right)^2 \tag{2}$$

The equation above can be rewritten in the form $\sigma_{\text{FS}}(\beta = 180°) = G \cdot S_B$, where $G = 4\pi \cdot \frac{S_B}{\lambda^2}$ is the directivity factor of the object in its shadow region.

Thus, the FSCS parameter is G times greater than the shadow area S_B of the target and is typically much larger than the monostatic RCS when the wavelength is significantly smaller than the cross-sectional (shadow) area of the target ($\lambda^2 \ll S_B$).

The phenomenon of forward scattering is best considered in the context of EM scattering mechanisms within three spatial regions:

1. The optical scattering region (optical domain), where the electrical dimensions of the object or target significantly exceed the wavelength – that is, the geometric dimensions D of the object/target satisfy $\frac{D}{\lambda} \gg 1$ or $D \gg \lambda$;
2. The Mie scattering region (Mie resonance region), where $\frac{D}{\lambda} \sim 1$;
3. The Rayleigh scattering region, where $\frac{D}{\lambda} \ll 1$ or $D \ll \lambda$.

Most of the existing studies on FSR are focused on the optical region and the upper part of the Mie resonance region [1]. In [3], it is shown that the maximum FSR effect occurs under the condition that:

$$0.5 < D/\lambda < 1.5 \tag{3}$$

This study focuses on the analysis of the forward scattering phenomenon in the context of detecting low-signature UAVs through numerical full-wave simulation using the HFSS environment. Various geometric shapes were selected as test objects, representing structural elements of UAVs – including a cylinder, a parallelepiped, and an ogive-shaped body (a streamlined aerodynamic form with smooth curvature, commonly used to describe the nose sections of UAVs and missiles).

The simulation results of the FSCS are presented for the case of a plane wave incident on a cylinder with a length of $L = 200$ cm and a diameter of $D = 30$ cm. The cylinder's surface is modeled as a perfect electric conductor (PEC) and is illuminated from above at frequencies of 100 MHz ($\lambda = 3$ m), 1 GHz ($\lambda = 30$ cm), and 5 GHz ($\lambda = 6$ cm). The EM illumination is configured such that the backscattering direction corresponds to an azimuth angle of 0° (positive Z-axis), while the FS direction corresponds to an azimuth angle of 180° (negative Z-axis) (see Fig. 2). The air box is defined relative to the surface of the cylinder, with a minimum distance of at least $\frac{\lambda}{4}$ from the cylinder. The maximum mesh element size (tetrahedrons) on the boundaries of the simulation domain is set to $\frac{\lambda}{5}$.

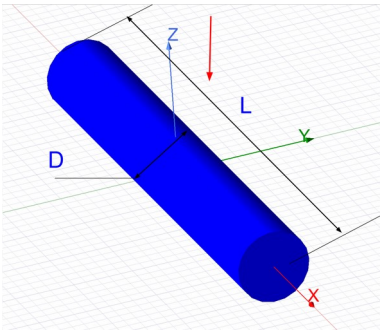

Fig. 2. Cylinder model and direction of incident plane wave propagation

The simulation results correspond to: the upper boundary of the Rayleigh–Mie scattering region (the Mie resonance region, where $\frac{D}{\lambda} \sim 1$ or $D \sim \lambda$), as shown in Fig. 3 (a, b), and to the optical scattering region (where $\frac{D}{\lambda} > 1$ or $D \gg \lambda$), as shown in Fig. 3 (c), respectively.

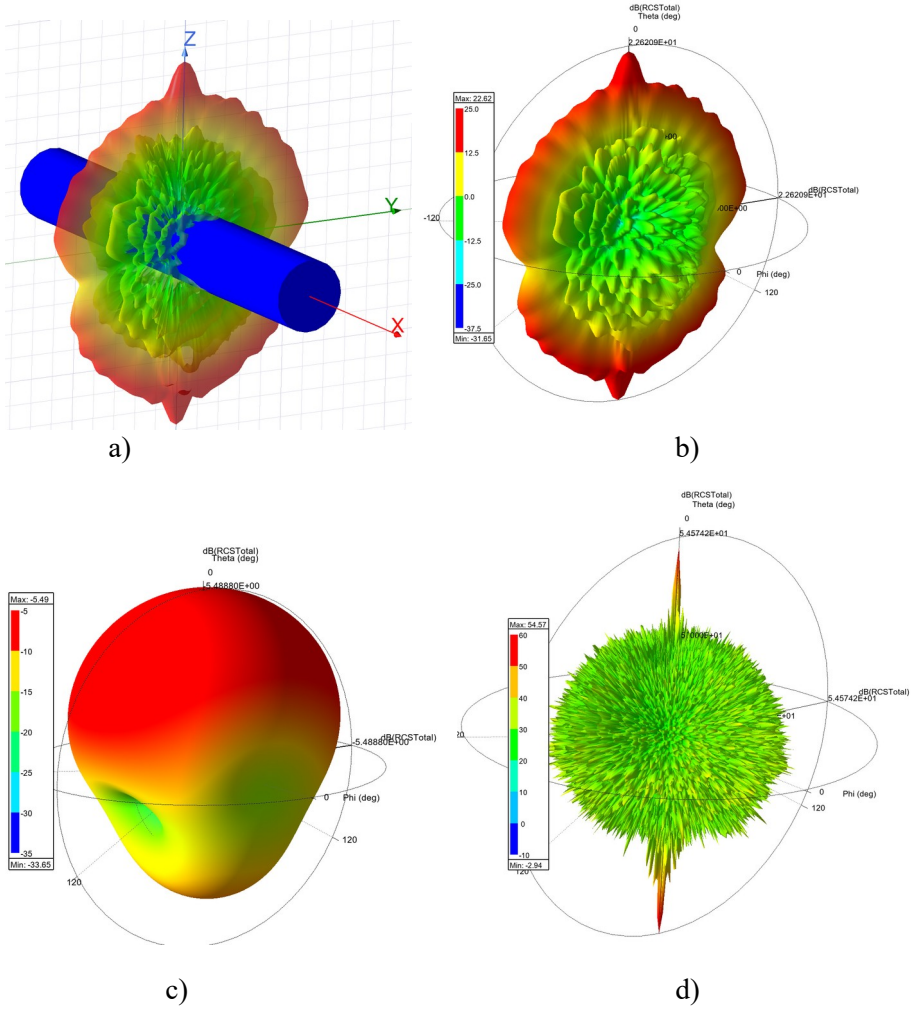

a) b)

c) d)

Fig. 3. Bistatic RCS (FSCS) radiation patterns for a cylinder at the following frequencies: 1 GHz (a, b), 100 MHz (c), and 5 GHz (d)

Figure 4 presents comparative RCS radiation patterns in the angular plane for a cylinder-type body at different frequencies. As the frequency increases, the signature of the cylindrical object becomes more

pronounced, and under plane-wave EM illumination at 5 GHz, the signal level in the FS direction reaches up to 54 dB.

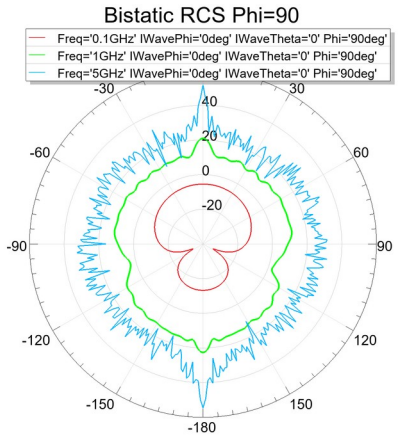

Fig. 4. RCS radiation patterns in the angular plane for a cylinder-type body at different frequencies

FSCS modeling was carried out for the case of a plane wave incident on a parallelepiped with dimensions $a = 200$ cm, $b = 200$ cm, and thicknesses $D = 3$ cm, 30 cm, and 50 cm. The surface of the model was defined as a perfect electric conductor (PEC). Illumination was performed at three elevation angles: $\theta = 0°$, 45°, and 90°, at a frequency of 1 GHz ($\lambda = 30$ cm). The air box was defined at a minimum distance of $\frac{\lambda}{4}$ from the surface of the parallelepiped. The maximum size of the tetrahedral mesh elements on the boundaries of the simulation domain was set to $\frac{\lambda}{5}$. The parallelepiped model is shown in Fig. 5.

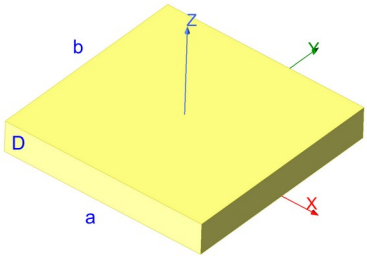

Fig. 5. Parallelepiped model

The simulation results are presented in Figs. 6 and 7. The plots show that significant RCS values are observed even outside the range defined by (3). However, the lobes that visually resemble an FSR structure are, in fact, formed by a different mechanism and do not represent the classical FSR effect. When $\frac{D}{\lambda}$ significantly exceeds 1, the object enters the optical (geometrical) scattering region, where dominant contributions arise from reflections off large flat surfaces and multimode edge diffractions from the long edges of the parallelepiped. The interference of these components produces a complex multi-lobe pattern that may resemble the shape of an FSR lobe, but is not related to the shadow diffraction that underlies the classical FSR phenomenon. Thus, beyond the range of $\frac{D}{\lambda} \approx 1$, the observed scattering is not true forward scattering, but rather a combination of specular reflections and edge diffractions characteristic of electrically large objects [4].

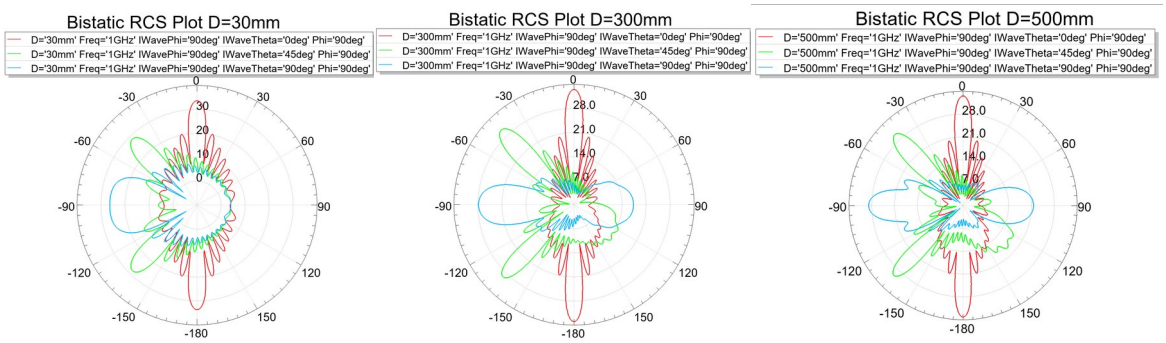

a) b) c)

Fig. 6. Bistatic RCS of the parallelepiped for different thicknesses D at 1 GHz: (a) $D = 3$ cm; (b) $D = 30$ cm; (c) $D = 50$ cm. Illumination at $\varphi = 90°$ $\theta = 0°$; $45°$ (red curve), $90°$ (green curve), (blue curve)

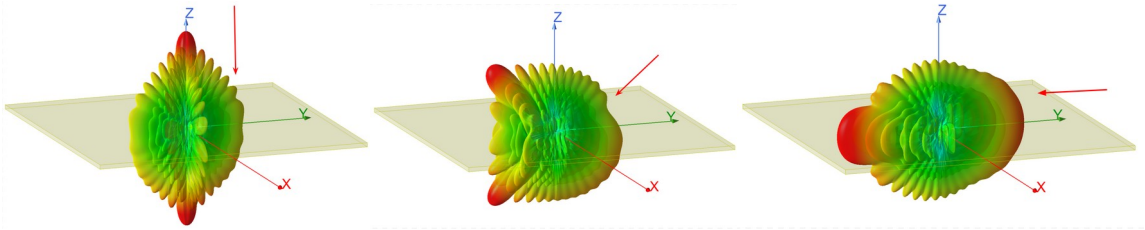

a) b) c)

Fig. 7. Bistatic RCS radiation patterns of the parallelepiped ($a = 200$ cm, $b = 200$ cm, $D = 30$ cm) under illumination at angles: (a) $\theta = 0°$; (b) $\theta = 45°$; (c) $\theta = 90°$ (indicated by the red arrow), at a frequency of 1 GHz ($\lambda = 30$ cm)

The next object under consideration is an ogive-shaped body (Fig. 8) with a cross-sectional diameter of cm and a length of cm, which more closely resembles real aerodynamic targets. The surface of the model is also defined as a perfect electric conductor (PEC) and is illuminated from above (indicated by the red arrow in Fig. 8) at frequencies of 100 MHz ($\lambda = 3$ m), 1 GHz ($\lambda = 30$ cm), and 5 GHz ($\lambda = 6$ cm). The EM illumination is configured such that the backscattering direction corresponds to an elevation angle of 0° (positive Z-axis), while the FS direction corresponds to an elevation angle of 180° (negative Z-axis). The air box is defined at a minimum distance of $\frac{\lambda}{4}$ from the surface of the ogive. The maximum size of the tetrahedral mesh elements on the boundaries of the simulation domain is set to $\frac{\lambda}{5}$.

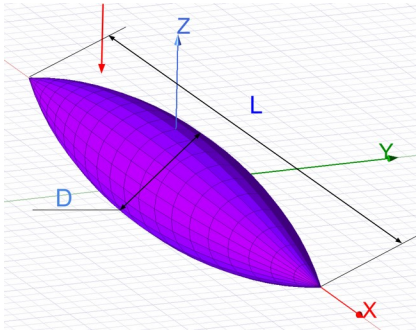

Fig. 8. Geometric model of the ogive-shaped body

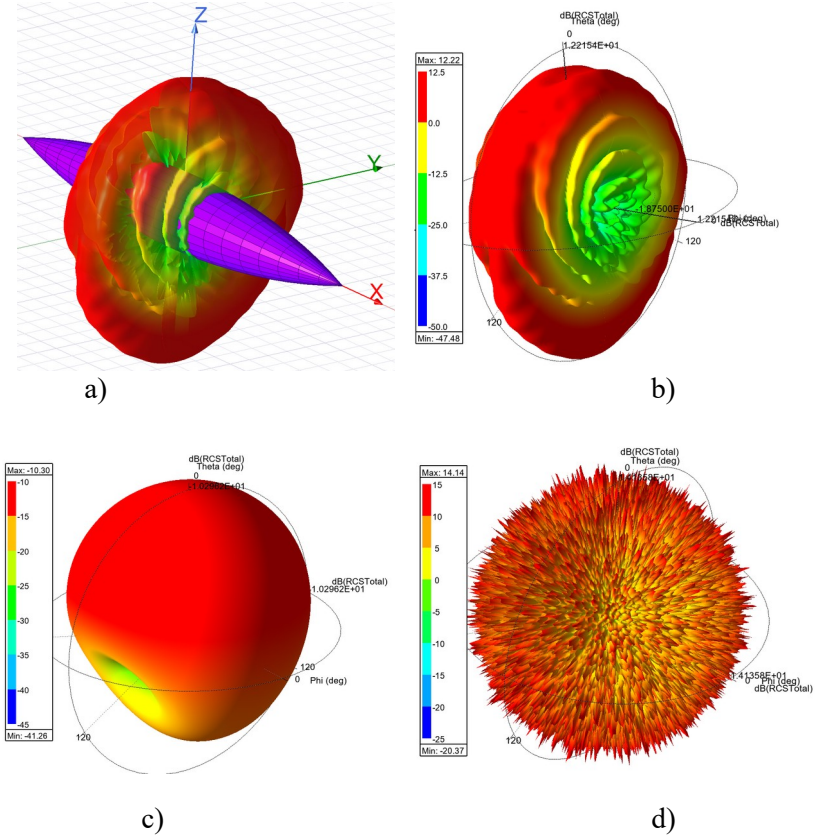

Fig. 9. Bistatic RCS radiation patterns of the ogive-shaped body at the following frequencies: 1 GHz (a, b), 100 MHz (c), and 5 GHz (d)

Figure 10 presents comparative RCS radiation patterns in the angular plane for the ogive-shaped body at different frequencies. At 1 GHz and 5 GHz, the presence of the object is not apparent in the RCS radiation patterns.

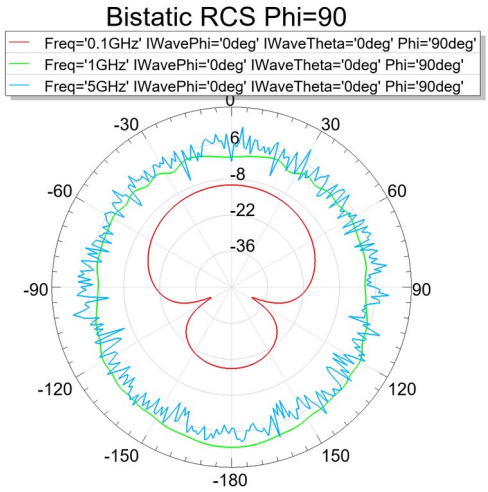

Fig. 10. RCS radiation patterns in the angular plane for the ogive-shaped body at different frequencies

Conclusions: The performed full-wave simulation has demonstrated that the FSR regime provides significant enhancement of the FSCS for small-sized objects, making it particularly sensitive to UAVs

and other low-signature targets. The FSR effect is primarily governed by the geometric shadow area of the object and is largely independent of material properties or stealth technologies. As a result, even small UAVs made of composite materials generate a strong diffraction FS peak in the 180° direction. For streamlined ogive-shaped bodies, the condition $0.5 < \frac{D}{\lambda} < 1.5$ is fully satisfied, ensuring a well-defined forward scattering response. In contrast, flat-shaped objects at large $\frac{D}{\lambda}$ ratios transition into the optical scattering regime, dominated by specular reflections. Thus, FSR is an effective and promising method for detecting small UAVs, including targets with low radar visibility, and can be implemented even using low-cost SDR receivers as part of passive radar systems.

Literature

1. Gashinova M., Daniel L., Myakinkov A., Cherniakov M. Forward Scatter Radar. У: Novel Radar Techniques and Applications. Vol. 1. Institution of Engineering and Technology (IET), 2018, pp. 563–619. DOI: 10.1049/SBRA512F_ch13.

2. Krzysztof Kulpa, Piotr Samczyński, Piotr Krysikю Forward Scattering Effect Exploitation in Passive Radars. Warsaw University of Technology, 2018.

3. Siegel, K.M. Bistatic radar cross sections of surfaces of revolution. Journal of Applied Physics, 26(1):297–305, 1955.

4. Ruck G.T., Barrick D.E., Stuart W.D., Jessen C.K. *Radar Cross Section Handbook. Vol. 1.* New York: Plenum Press, 1970.